

Retrieval of multiple scattering contrast from x-ray analyzer-based imaging

Heng Chen(陈恒), Bo Liu(刘波), Li-Ming Zhao(赵立明), Kun Ren(任坤), and Zhi-Li Wang(王志立)

Citation: Chin. Phys. B, 2021, 30 (**1**): 018701. DOI: 10.1088/1674-1056/abbbed
Journal homepage: http://cpb.iphy.ac.cn; http://iopscience.iop.org/cpb

What follows is a list of articles you may be interested in

Biases of estimated signals in x-ray analyzer-based imaging

Jianlin Xia(夏健霖), Wen Xu(徐文), Ruicheng Zhou(周瑞成), Xiaomin Shi(石晓敏), Kun Ren(任坤), Heng Chen(陈恒), Zhili Wang(王志立)
Chin. Phys. B, 2020, 29 (**6**): 068703. DOI: 10.1088/1674-1056/ab8887

Theory and method of dual-energy x-ray grating phase-contrast imaging

Feng Rong(荣锋), Yan Gao(高艳), Cui-Juan Guo(郭翠娟), Wei Xu(徐微), Wei Xu(徐伟)
Chin. Phys. B, 2019, 28 (**10**): 108702. DOI: 10.1088/1674-1056/ab3f1d

Shifting curves based on the detector integration effect for x-ray phase contrast imaging

Jun Yang(杨君), Jin-Chuan Guo(郭金川), Yao-Hu Lei(雷耀虎), Ming-Hao Yi(易明皓), Li Chen(陈力)
Chin. Phys. B, 2017, 26 (**2**): 028701. DOI: 10.1088/1674-1056/26/2/028701

Elemental x-ray imaging using Zernike phase contrast

Qi-Gang Shao(邵其刚), Jian Chen(陈健), Faiz Wali, Yuan Bao(鲍园), Zhi-Li Wang(王志立), Pei-Ping Zhu(朱佩平), Yang-Chao Tian(田扬超), Kun Gao(高昆)
Chin. Phys. B, 2016, 25 (**10**): 108702. DOI: 10.1088/1674-1056/25/10/108702

Simple phase extraction in x-ray differential phase contrast imaging

Xin Liu(刘鑫), Jin-Chuan Guo(郭金川), Yao-Hu Lei(雷耀虎), Ji Li(李冀), Han-Ben Niu(牛憨笨)
Chin. Phys. B, 2016, 25 (**2**): 028704. DOI: 10.1088/1674-1056/25/2/028704

Retrieval of multiple scattering contrast from x-ray analyzer-based imaging*

Heng Chen(陈恒), Bo Liu(刘波), Li-Ming Zhao(赵立明), Kun Ren(任坤), and Zhi-Li Wang(王志立)†

School of Electronics Science & Applied Physics, Hefei University of Technology, Hefei 230009, *China*

(Received 6 June 2020; revised manuscript received 2 September 2020; accepted manuscript online 28 September 2020)

We present a moment-based alternative approach to retrieve multiple scattering contrasts from x-ray analyzer-based imaging. By use of the properties of moments of convolutions, the multiple-image radiography approach is theoretically validated. Furthermore, higher order moments of the object scattering distribution, inaccessible in multiple-image radiography, are simultaneously provided by this alternative approach. It is experimentally demonstrated that the skew and kurtosis information related to the distribution of sub-pixel features within the object can be obtained from those complementary contrasts. Finally, the sensitivity of the retrieved multiple scattering contrasts is investigated experimentally. The finding that the sensitivity is inversely proportional to the square root of the detected photon number essentially indicates that the retrieval of moments with an order higher than two can be achieved without increasing exposure time or dose. The presented alternative approach provides an access to the exploitation of multiple scattering contrasts, which is expected to be useful in biomedical research, materials science, security screening, *etc*.

Keywords: x-ray imaging, analyzer-based imaging, rocking curve, moment analysis

PACS: 87.59.–e, 42.30.Va, 41.50.+h, 87.57.N– **DOI:** 10.1088/1674-1056/abbbed

1. Introduction

X-ray refraction and scattering imaging have been demonstrated to provide complementary information to conventional attenuation-based radiography and computed tomography.[1] In x-ray analyzer-based imaging (ABI), the attenuation, refraction (*i.e.*, differential phase contrast), and scattering signals are measured simultaneously by using an analyzer crystal.[2] The high angular sensitivity of the rocking curve (RC) of the analyzer crystal enables the detection of small changes in the x-ray propagation direction after the x-ray has interacted with a sample. While the refraction signal features improved soft-tissue contrast,[1] the scattering signal enables the visualization of microstructures below the imaging resolution limit.[3] Over the last decades, the great potential of x-ray analyzer-based imaging has been explored, including, but not limited to, breast and cartilage imaging,[4] quantification of microbubble concentration,[5] functional lung imaging,[6] *in situ* analysis of damage evolution,[7] and non-invasive soft tissue engineering.[8]

In x-ray analyzer-based imaging, the contrast in the acquired projection images is given by a mixture of attenuation, refraction, and ultra-small-angle x-ray scattering (USAXS) information. This signal superposition makes the image interpretation ambiguous in many practical applications. Therefore, several approaches to separate the three different signals and accurately quantify them have been developed.[9–16] Among the existing approaches, multiple-image radiography (MIR) has the advantage of being stable against the noise, and therefore it can be widely used in various fields.[4–8] The MIR is based on the assumption that for each detector pixel, the measured angular distribution of the diffracted intensity results from the convolution of the reference RC with the object's scattering distribution.[10,13] Consequently, one calculated the zeroth-, first-, and second-order moments of the rocking curve pixel-by-pixel, and deduced that the attenuation is the ratio of the zeroth-order moment of the object RC to that of the reference RC, the refraction the difference between the first-order moment of the object RC and that of the reference RC, and the USAXS difference between the second-order moment of the object and that of the reference RC.[9,10] However, to the best of our knowledge, there still remains a lack of theoretical foundation for the MIR approach. While the relation that links the attenuation, refraction, and USAXS signals to the moments of object scattering distributions has been theoretically derived,[17] it is unclear in theory how the moments of the object scattering distribution are related to their counterparts of the object RC and reference RC. Furthermore, MIR does not exploit the additional information provided by the moments with an order higher than two. That information can be valuable for a comprehensive understanding of the distribution of sub-pixel features within the object. While the skew and kurtosis images were reported in x-ray grating interferometry and edge illumination,[18–21] no such images have been reported in x-ray analyzer-based imaging yet.

In this work, we present an alternative approach to re-

*Project supported by the National Natural Science Foundation of China (Grant Nos. 11475170, U1532113, and 11905041) and the Fundamental Research Funds for the Central Universities, China (Grant No. PA2020GDKC0024).

†Corresponding author. E-mail: dywangzl@hfut.edu.cn

© 2021 Chinese Physical Society and IOP Publishing Ltd

trieve multiple scattering contrasts from x-ray analyzer-based imaging. This technique is inspired by a similar approach in edge illumination (EI).[21] The x-ray ABI and EI are sensitive to the same physical quantities and thus share parallels in some aspect of measurement and signal retrieval.[15,22] By use of the properties of the moments of convolutions, the relations between the moments of the object scattering distribution and those of measured object RC and reference RC are identified theoretically. It not only validates the MIR algorithm, but also provides an access to additional structural information, which is demonstrated through the proof-of-principle experiments. Finally, we investigate experimentally the dependence of the sensitivity of retrieved multiple scattering contrast on the detected photon number.

2. Retrieval of multiple scattering contrasts from x-ray analyzer-based imaging

Consider the typical x-ray ABI system schematically shown in Fig. 1, where a parallel, monochromatic x-ray beam is created by the first crystal, transmitted through the object and diffracted by the second analyzer crystal. Owing to the narrow angular range of Bragg diffraction, the analyzer crystal efficiently selects the rays locally deviated by a specific angular amount, thus enhancing the image contrast. The observed intensity modulation at the detector is described by the rocking curve, which varies with the angular position of the analyzer crystal.

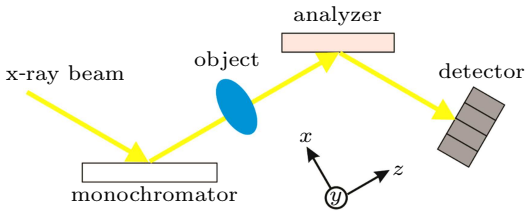


Fig. 1. Schematic diagram of the x-ray ABI system.

In x-ray ABI experiments, scanning the analyzer crystal with and without the object provides the object RC $I(\theta)$ and the reference RC $R(\theta)$ for each detector pixel, respectively. In theory, the measured object RC $I(\theta)$ can be modelled by the convolution of the reference RC $R(\theta)$ with the object's scattering distribution $f(\theta)$ as follows:[10,13]

$$I(\theta) = R(\theta) \otimes f(\theta), \tag{1}$$

where $\otimes$ denotes the convolution operator. The object scattering distribution is determined by the sub-pixel structure within the object.

In the following, we propose an alternative data analysis approach in order to retrieve multiple contrasts relating to the properties of $f(\theta)$. In this novel approach, a moment analysis is applied to the measured angularly resolved intensities. For this, the following definitions of the moments can be distinguished. For an arbitrary function $h(\theta)$, the algebraic moment is defined by

$$M_n(h) = \int \theta^n h(\theta)\,\mathrm{d}\theta, \tag{2}$$

where the integer n denotes the order of the moment. Dividing $M_n(h)$ by M_0 leads to the normalized algebraic moments as follows:

$$\bar{M}_n(h) = M_n(h)/M_0(h) \quad (n \geq 1), \tag{3}$$

and further shifting $\bar{M}_n(h)$ by $\bar{M}_1$ yields the normalized central moments

$$\tilde{M}_n(h) = \int (\theta - \bar{M}_1)^n h(\theta)\,\mathrm{d}\theta / M_0 \quad (n \geq 2). \tag{4}$$

It has been experimentally demonstrated that the ratio $M_0(I)/M_0(R)$, the difference $\bar{M}_1(I) - \bar{M}_1(R)$, and the difference $\tilde{M}_2(I) - \tilde{M}_2(R)$ correspond to the object's attenuation, refraction, and scattering width, respectively.[9,18,21]

As shown in Eq. (1), the measured object RC is the convolution of the reference RC with the object's scattering distribution for each detector pixel, and therefore its Fourier transform is given by

$$I(\theta) = R(\theta) \otimes f(\theta) \Leftrightarrow \hat{I} = \sqrt{2\pi} \cdot \hat{R} \cdot \hat{f}, \tag{5}$$

where the symbol $\hat{}$ denotes the Fourier transform. Based on Eq. (5), the proposed approach further makes use of the characteristic property of the moments of convolutions. In Fourier space, the n-th algebraic moment defined in Eq. (2) is directly related to the n-th derivative at zero frequency by[23]

$$M_n(I) = \frac{\sqrt{2\pi}}{(-\mathrm{i})^n} \left.\frac{\mathrm{d}^n \hat{I}}{\mathrm{d}q^n}\right|_{q=0} \tag{6}$$

with q being the variable in Fourier space. By substituting Eq. (5) into Eq. (6), and dividing the resulting equation by $M_0(I)$, we obtain

$$\bar{M}_n(I) = \sum_{k=0}^{n} C_n^k \bar{M}_k(R)\,\bar{M}_{n-k}(f), \tag{7}$$

where C_n^k is the binomial coefficient. Since the moment of I and R can be calculated respectively from object measurement and reference measurement, equation (7) provides a direct access to multiple moment of the object scattering distribution f. The relations of these moments to the object properties have already been derived in the literature.[17] Specifically, the results for the first five moments are given by

$$M_0(f) = M_0(I)/M_0(R), \tag{8}$$

$$\bar{M}_1(f) = \bar{M}_1(I) - \bar{M}_1(R), \tag{9}$$

$$\tilde{M}_2(f) = \tilde{M}_2(I) - \tilde{M}_2(R), \tag{10}$$

$$\tilde{M}_3(f) = \tilde{M}_3(I) - \tilde{M}_3(R), \tag{11}$$

$$\tilde{M}_4(f) = \tilde{M}_4(I) - \tilde{M}_4(R) - 6\tilde{M}_2(R)\left[\tilde{M}_2(I) - \tilde{M}_2(R)\right]. \tag{12}$$

Note that equations (8)–(12) are the main contributions of this work. On the one hand, equations (8)–(10) identify the relations between the moments of the object scattering distribution and those of the measured object RC and reference RC, and therefore can be considered as the theoretical verification of the MIR algorithm. On the other hand, the access to moments with an order higher than two provides additional structural information about the investigated object on a sub-pixel scale. While the third-order moment in Eq. (11) is related to the skew information that quantifies the asymmetry of the scattering distribution, equation (12) enables the retrieval of the kurtosis that is a measure of tail strength of the scattering distribution. Note that these scattering contrasts are previously unobtainable in the MIR approach.

3. Experimental results

To demonstrate the potential applications of multiple scattering contrasts, experiments on synchrotron radiation are performed by using the 4W1A beamline of Beijing Synchrotron Radiation Facility.[24] The x-rays with a photon energy of 15 keV are selected by the first Si (111) monochromator crystal, and the second Si (111) crystal is used to analyze the x-ray beam exiting from the sample. The intensity is recorded by use of a high-resolution x-ray digital camera system FDS694 designed by Photonic Science Ltd, with a pixel size of 4.5 μm. For both the object scan and the reference scan, intensities are measured at 61 angular positions of the analyzer crystal, ranging from −60 μrad to 60 μrad in steps of 2 μrad. The dark-field images are also acquired and averaged. Prior to image processing, the averaged dark-field image is subtracted from both the object image and the reference image. The exposure time is 70 ms for each image.

For this proof-of-principle experiment, we adopt some kind of ladybird as a biological sample, which contains a variety of features with different size scales. Figures 2(a)–2(c) show the retrieved attenuation $(i.e., -\log[M_0(f)])$ image, the refraction image, and the USAXS width $\left(i.e., \sqrt{\tilde{M}_2(f)}\right)$ image of a ladybird, respectively. The refraction image and the USAXS width image are displayed in units of microradians. While the skeletal structure can be clearly identified in the conventional attenuation image, the interfaces between features of different densities or geometrical shapes inside the sample produce much stronger signals in the refraction and/or USAXS width image. These results serve as an illustration of the complementarity of three different imaging modalities.

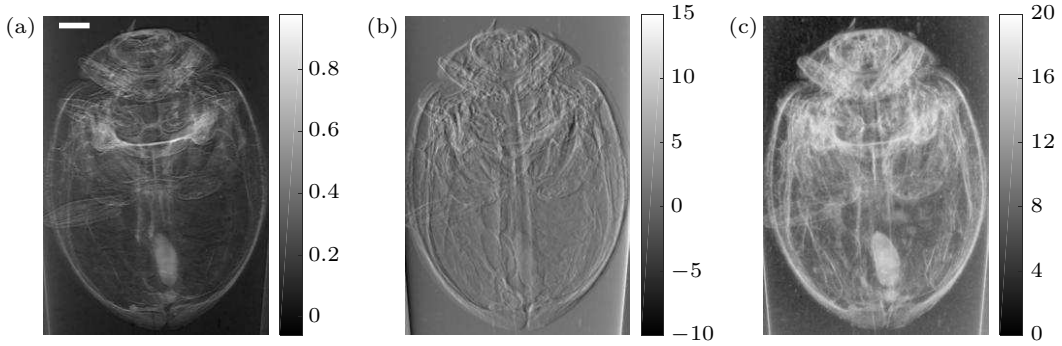


Fig. 2. Image of (a) attenuation, (b) refraction, and (c) USAXS width of the ladybird, with scale bar being 450 μm in panel (a).

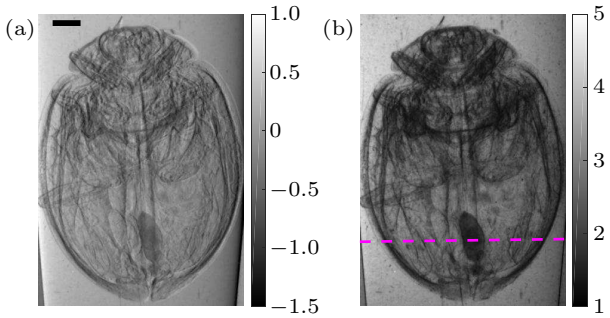


Fig. 3. (a) Skew and (b) kurtosis of scattering distributions of the ladybird, with scale bar being 450 μm in panel (a).

Furthermore, the skewness and the kurtosis of the scattering distribution of the ladybird are obtained from the same experimental data set, and the resulting images are displayed in Figs. 3(a) and 3(b), respectively, as a demonstration of previously inaccessible information provided by higher order moments. The skewness S is calculated from[23]

$$S = \tilde{M}_3(f) \Big/ \left[\sqrt{\tilde{M}_2(f)}\right]^3, \tag{13}$$

the value of which is negative when the negative tail is longer than the positive one, and *vice versa* for positive values. The kurtosis κ, which quantifies the weight of the tails compared with the central peak, is determined from[23]

$$\kappa = \tilde{M}_4(f) / \left[\tilde{M}_2(f)\right]^2. \tag{14}$$

These contrast images, inaccessible by the standard MIR approach, indeed provide an additional insight into the sub-pixel features within the object. Note that the results shown in Fig. 3 are directly calculated by use of Eqs. (13) and (14), without any further image processing.

Moreover, a comparison between Fig. 3(b) and Fig. 2(c) shows that the previously unobtainable kurtosis provides complementary information to MIR approach. For further demonstration, figure 4 shows the line profiles of the USAXS width and kurtosis image at the position indicated by the dashed line in Fig. 3(b). The complementarity of the kurtosis image to the USAXS width image is clearly illustrated, where a pixel with a small USAXS width has a large value of the kurtosis. Therefore, motivated by the proof-of-principle experimental results, we can expect that the simultaneous retrieval of multiple scattering contrasts, with the access to additional information about sub-pixel features of the object, could have diverse applications, such as materials science. Besides, it is mentioned that different assumptions about the object scattering distribution were made by information retrieval methods reported previously.[13–16] However, the proposed approach in the present work does not assume a specific shape of the measured RC and, thus providing the reliable results for arbitrarily shaped scatter distributions.

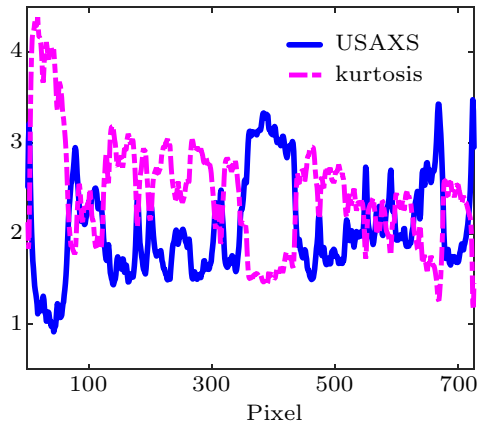


Fig. 4. Line profile of USAXS width image and kurtosis image of ladybird.

Finally, we investigate the dependence of the sensitivities of the retrieved multiple scattering contrasts on the incident photon number. An additional dataset is acquired for this purpose. As a quantitative measure of the sensitivity, we use the standard deviation of the retrieved distinct scattering contrasts from a background region of 50×50 pixels. As shown in Fig. 5, the logarithm of the standard deviations of different moments of the scattering distributions is plotted as a function of the logarithm of the detected photon number, together with the least-squares fitting. As can be seen, given a constant photon number, the sensitivity of the zero-order moment is the highest, and that of the fourth-order moment is the lowest. This observation is within our expectation. Furthermore, the linear dependence is found for all the first five moments of the scattering distribution, with the fitted slope being −0.4857 for M_0, −0.4937 for $\tilde{M}_1$, −0.5192 for $\tilde{M}_2$, −0.5221 for $\tilde{M}_3$, and −0.5179 for $\tilde{M}_4$, respectively. These results indicate that the sensitivities of the obtained multiple scattering contrasts are approximately inversely proportional to the square root of the photon number. Essentially, this fact means that the moment analysis approach provides the additional and complementary scattering contrasts (*i.e.*, moments with an order higher than two) without the need of extra exposure time or dose.

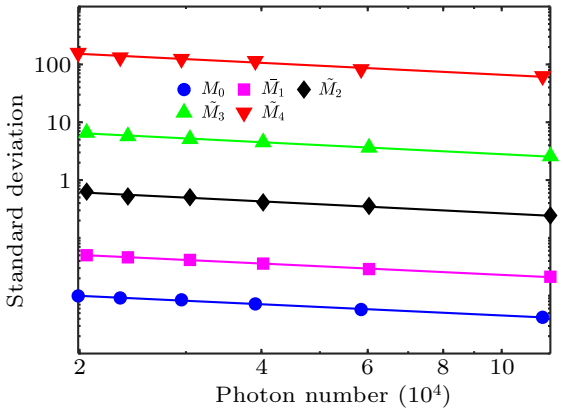


Fig. 5. Log–log plots of sensitivities of the first five moments of scattering distribution *versus* detected photon number, together with the least-squares fitting.

4. Conclusions

In this work, we present an alternative approach to retrieve the multiple scattering contrasts from x-ray analyzer-based imaging. This novel approach is based on the well-established image formation model, and makes use of the properties of the moments of convolutions. By a direct moment analysis, the working principle of multiple-image radiography is theoretically verified. It is demonstrated by proof-of-principle experiments that higher-order moments of the scattering distributions are simultaneously provided by this alternative approach. Those complementary contrasts provide access to additional information about sub-pixel features within the object, and are not accessible by multiple-image radiography. Finally, we experimentally demonstrate that the sensitivities of retrieved multiple scattering contrasts are all inversely proportional to the square root of the detected photon number. These preliminary results suggest the great potential for the applications of additional scattering contrasts in biomedical research, materials science, security screening, *etc*. The moment analysis approach can also be generalized to two-dimensional x-ray analyzer-based imaging.[25]

References

[1] Bravin A, Coan P and Suortti P 2013 *Phys. Med. Biol.* **58** R1
[2] Diemoz P C, Coan P, Glaser G and Bravin A 2010 *Opt. Express* **18** 3494
[3] Yashiro W, Terui Y, Kawabata K and Momose A 2010 *Opt. Express* **18** 16890

[4] Suortti P, Keyriläinen J and Thomlinson W 2013 *J. Phys. D: Appl. Phys.* **46** 494002
[5] Millard T P, Endrizzi M, Rigon L, Arfelli F, Menk R H, Owen J, Stride E and Olivo A 2013 *Appl. Phys. Lett.* **103** 114105
[6] Aulakh G K, Mann A, Belev G, Wiebe S, Kuebler W M, Singh B and Chapman D 2018 *Phys. Med. Biol.* **63** 015009
[7] Nellesen J, Laquai R, Müller B R, Kupsch A, Hentschel M P, Anar N B, Soppa E, Tillmann W and Bruno G 2018 *J. Mater. Sci.* **53** 6021
[8] Izadifar Z, Honaramooz A, Wiebe S, Belev G, Chen X B and Chapman D 2016 *Biomaterials* **82** 151
[9] Pagot E, Cloetens P, Fiedler S, Bravin A, Coan P, Baruchel J, Härtwig J and Thomlinson W 2003 *Appl. Phys. Lett.* **82** 3421
[10] Wernick M N, Wirjadi O, Chapman D, Zhong Z, Galatsanos N P, Yang Y, Brankov J G, Oltulu O, Anastasio M A and Muehleman C 2003 *Phys. Med. Biol.* **48** 3875
[11] Rigon L, Arfelli F and Menk R H 2007 *Appl. Phys. Lett.* **90** 114012
[12] Nesterets Y I, Coan P, Gureyev T E, Bravin A, Cloetens P and Wilkins S W 2006 *Acta Cryst. A* **62** 296
[13] Majidi K, Li J, Muehleman C and Brankov J G 2014 *Phys. Med. Biol.* **59** 1877
[14] Yang H, Xuan R J, Hu C H and Duan J H 2014 *Chin. Phys. B* **23** 048701
[15] Wang Z L, Liu D L, Zhang J, Huang W X, Yuan Q X, Gao K and Wu Z 2018 *J. Synchrotron Rad.* **25** 1206
[16] Aefelli F, Astolfo A, Rigon L and Menk R H 2018 *Sci. Rep.* **8** 362
[17] Modregger P, Kagias M, Irvine S C, Brönnimann R, Jefimovs K, Endrizzi M and Olivo A 2017 *Phys. Rev. Lett.* **118** 265501
[18] Modregger P, Scattarella F, Pinzer B R, David C, Bellotti R and Stampanoni 2012 *Phys. Rev. Lett.* **108** 048101
[19] Modregger P, Rutishauser S, Meiser J, David C and Stampanoni 2014 *Appl. Phys. Lett.* **105** 024102
[20] Modregger P, Cremona T P, Benarafa C, Schittny J C, Olivo A and Endrizzi M 2016 *Sci. Rep.* **6** 30940
[21] Modregger P, Endrizzi M and Olivo A 2018 *Appl. Phys. Lett.* **113** 254101
[22] Endrizzi M, Diemoz P C, Millard T P, Louise Jones J, Speller R D, Robinson I K and Olivo A 2014 *Appl. Phys. Lett.* **104** 024106
[23] James F 2006 *Statistical Methods in Experimental Physics*, 2nd edn. (Singapore: World Scientific Publishing Co. Pte. Ltd.)
[24] Yuan Q X, Zhang K, Hong Y L, Huang W X, Gao K, Wang Z L, Zhu P P, Gelb J, Tkachuk A, Hornberger B, Feser M, Yun W B and Wu Z Y 2012 *J. Synchrotron Rad.* **19** 1021
[25] Modregger P, Lübbert D, Schäfer P and Köhler R 2007 *Appl. Phys. Lett.* **90** 193501